Amino Acid Oxidation of Candida antarctica Lipase B Studied by Molecular Dynamics Simulations and Site-Directed Mutagenesis

Irani, Mehdi; Törnvall, Ulrika; Genheden, Samuel; Wittrup Larsen, Marianne; Hatti-Kaul, Rajni; Ryde, Ulf

Published in:
Biochemistry

DOI:
10.1021/bi301298m

2013

Amino acid oxidation of *Candida antarctica* lipase B studied by molecular dynamics simulations and site-directed mutagenesis

Mehdi Irani [1,2], Ulrika Törnvall [3,4], Samuel Genheden [1],

Marianne Wittrup Larsen [5], Rajni Hatti-Kaul [3], Ulf Ryde *[1]

[1] Department of Theoretical Chemistry, Lund University, Chemical Centre, P. O. Box 124, SE-221 00 Lund, Sweden

[2] Current address: Department of Chemistry, University of Kurdistan, Sanandaj, Iran

[3] Department of Biotechnology, Lund University, Chemical Centre, P. O. Box 124, SE-221 00 Lund, Sweden

[4] Current address: Center for Process Engineering and Technology, Department of Chemical and Biochemical Engineering, Technical University of Denmark, 2800 Lyngby, Denmark

[5] Department of Biochemistry, School of Biotechnology, Royal Institute of Technology, AlbaNova University Center, 106 91 Stockholm, Sweden

Correspondence to Ulf Ryde, E-mail: Ulf.Ryde@teokem.lu.se,

Tel: +46 – 46 2224502, Fax: +46 – 46 2228648

2014-01-03

Abstract

Molecular dynamics simulations have been performed on the lipase B from *Candida antarctica* (CalB) in its native form and with one or two oxidised residues, either methionine oxidised to methionine sulphoxide, tryptophan oxidised to 5-hydroxytryptophan, or cystine oxidised to a pair of cysteic acid residues. We have analysed how these mutations affect the general structure of the protein, as well as the local structure around the oxidised amino acid and the active site. The results indicate that the methionine and tryptophan oxidations led to rather restricted changes in the structure, whereas the oxidation of cystines, which also caused cleavage of the cystine S–S linkage, gave rise to larger changes in the protein structure. Only two oxidised residues caused significant changes in the structure of the active site, viz. those of the Cys-22/64 and Cys-216/258 pairs. Site-directed mutagenesis studies were also performed. Two variants showed a similar behaviour as native CalB (M83I and M129L), whereas W155Q and M72S had severely decreased specific activity. M83I had a slightly higher thermostability than native CalB. No significant increase in stability towards hydrogen peroxide was observed. The same mutants were also studied by molecular dynamics. Even though no significant increase in stability towards hydrogen peroxide was observed, the results from simulations and site-directed mutagenesis give some clues to the direction of further work on stabilization.

Key Words: molecular dynamics, oxidised amino acids, epoxidation, lipase, single point mutations.

Introduction

Industrial biotechnology is an important tool for the chemical industry to facilitate a paradigm shift from fossil- to bio-based production, and also for providing selective and energy-efficient process alternatives to chemical synthesis. Despite many advantages of biocatalysis, one major limitation to its widespread application has been the access to suitable biocatalysts with respect to activity and stability under process conditions. Oxidation has been identified as one of the major degradation pathways in proteins and peptides, resulting in loss of activity.[1]

Epoxidation is among the most important reactions in organic chemistry. Epoxides are important building blocks in organic synthesis and provide a variety of industrially important products, e.g. polyurethane, cross-linkers for powder coatings, PVC-plasticisers and surfactants.[2,3,4] Different enzymes, including lipases, chloroperoxidases, cytochrome P450 monooxygenases, and epoxide hydrolases, have been used to catalyse epoxidation reactions, among which lipases have shown several promising features.[5,6,7] The reactions catalysed by peroxidases and lipases use hydrogen peroxide as the oxygen donor. Many lipases accept hydrogen peroxide as a nucleophile and catalyse the formation of peroxycarboxylic acids, from which one of the oxygen atoms is spontaneously transferred to the double bond of a substrate to form an epoxide,[8] as is shown in Figure 1.

Lipase B from the basidiomycetous yeast *Candida* (also called *Pseudozyma*) *antarctica* (CalB)[9] is one of the most widely used biocatalysts in industry.[10] The enzyme has a molecular weight of 33 kDa and a p*I* of 6.0. The structure of CalB has been resolved by X-ray diffraction.[11,12] The polypeptide chain is composed of 317 amino acids, which fold into a α/β hydrolase fold. Like other lipases, CalB is a serine hydrolase and the active site contains a Ser–His–Asp catalytic triad. However, unlike other lipases, CalB does not seem to possess a lid domain.[13] Furthermore, it has a limited amount of space available in the active-site pocket and thus exhibits a high degree of selectivity. CalB has three disulphide bridges and is glycosylated at Asn-74.[12] The enzyme has been expressed in *Aspergillus oryzae, Pichia pastoris*, and *Escherichia coli*.[14]

For use in organic synthesis, the enzyme is typically immobilized onto a solid matrix. An earlier study has shown immobilized CalB to be the most efficient lipase for the synthesis of peroxy acid.[6] This might be owing to a higher resistance of CalB to oxidation by hydrogen peroxide compared to the other lipases, which in turn could be related to a lower number of oxidation-sensitive amino acids in the enzyme. However, recently it has been shown that Novozym®435 (CalB adsorbed to an acrylic copolymer) becomes inactive during its use as a catalyst in epoxidation processes under solvent-free conditions[6] and that the rate of enzyme inactivation is related to the concentration of H_2O_2 and temperature.[15]

CalB has one His, four Met, five Trp, and eight Tyr residues, i.e. residues that could be expected to be sensitive to oxidation. In order to improve its stability, it is important to get an understanding of the effect of oxidation on the enzyme structure and dynamics. Recently, the oxidation of CalB with hydrogen peroxide has been investigated by mass spectrometry.[16,17] The results showed that Met-298 was most prone to oxidation. However, oxidation of the other three Met residues (Met-72, 83, and 129), two Trp residues (Trp-65 and 155), and all three disulphide bridges (Cys-22, 64, 216, 258, 293, and 311) was also detected (the location of the various oxidised residues are indicated in Figure 2). On the other hand, the active-site His residue was not oxidised. Extended exposure to H_2O_2 led to partial fragmentation of the back-bone and extensive changes in the structure of the protein.

A logical remedy to the oxidation damage of CalB is to replace amino acids that are easily oxidised by more resistant amino acids using mutagenesis. However, this is necessary only if the oxidations affect the structure or activity of the enzyme. Therefore, in this work we perform molecular dynamics (MD) simulations of CalB with various oxidised amino acids. The aim is to examine how the various oxidations affect the general structure of the protein, as well as the local structure of the active site. To further investigate the effect of oxidation, as

well as to verify the MD simulations, site-directed mutagenesis of CalB is also performed and the corresponding mutants are expressed and tested for activity and stability. The mutants are also studied by MD simulations.

Methods

Molecular dynamics simulations

The MD simulations were based on a 1.55 Å crystal structure of CalB (PDB id 1TCA).[11] The protein was solvated in a truncated octahedral box extending at least 9 Å on all sides of the protein, giving a total of 7988 water molecules and ~28 600 atoms. All Lys and Arg residues were assumed to be positively charged and all Asp and Glu residues were negatively charged. The only exception was Asp-134, which is deeply buried in the protein, close to the active site. It was modelled as protonated and neutral in all simulations, except one (WtD). This assignment was confirmed by the PROPKA software.[18] All six Cys residues were involved in disulphide linkages. The only His residue in CalB is His-224, which together with Ser-105 and Asp-187 constitute the catalytic triad. We studied the free enzyme without any bound substrate. Therefore, we assumed that Asp-187 was deprotonated, accepting a hydrogen bond from ND1 of His-224, whereas the NE2 atom was deprotonated and accepted a hydrogen bond from Ser-105 at the start of the simulations.

Sixteen different simulations were performed in this study: Two involved the native (wild-type) protein and they differed in the protonation state of Asp-134, protonated (WtP) or deprotonated (WtD). In ten simulations, Asp-134 was protonated and one or two amino acids were oxidised, viz. Met-72, 83, 129, 298, Trp-52, 65, 155, or the two Cys residues of the former disulphide bridges Cys-22 and 64, Cys-216 and 258, or Cys-293 and 311. These simulations will be denoted M72, M83, M129, M298, W52, W65, W155, C22/64, C216/258, and C293/311, respectively. The location and the solvent-accessibility of the various oxidised residues are indicated in Figure 2. In addition, four mutants were constructed, M72S, M83I, M129L, and W155Q, by cutting away the modified atoms and adding the new ones by the tleap module in Amber 10.[19] In all mutants, Asp-134 was protonated.

The simulations were started by a 240 ps simulated-annealing MD in which only the added water molecules and hydrogen atoms were allowed to move, while the temperature was first kept at 370 K and then slowly reduced to 0 K. It was followed by 10 000 steps of minimisation. Then, all atoms were allowed to move, the temperature was set to 300 K, and a 500 ps equilibration was run with a constant pressure (1 atm). Finally, a 18 ns production simulation was run with the same conditions. The C216/258 and C293/311 simulations showed extensive variation in some of the properties during these 18-ns simulations. Therefore, these simulations were extended to 33 ns and the analysis is based on the last 18 ns of the simulations.

All MD simulations were run using the sander module of Amber 10.[19] The temperature was kept constant at 300 K using Langevin dynamics[20] with a collision frequency of 2.0 ps^{-1} and the pressure was kept constant at 1 atm using a weak-coupling isotropic algorithm with a relaxation time of 1 ps.[21] Particle-mesh Ewald summation with a fourth-order B spline interpolation and a tolerance of 10^{-5} was used to handle the long-range electrostatics.[22] The cut-off for non-bonded interactions was set to 8 Å and the non-bonded pair list was updated every 50 fs. The SHAKE algorithm[23] was used to constrain bonds involving hydrogen atoms so that a 2 fs time step could be used.

The normal amino acids were described by the Amber 99SB force field[24] and water molecules with the TIP3P model.[25] Met was assumed to be oxidised to methionine sulphoxide, Cys to cysteic acid, and Trp to 5-hydroxytryptophan.[26] Charges for these residues were obtained by optimising the isolated side chains at the Hartree–Fock/6-31G* level of theory. Then, the electrostatic potential was calculated with the same method in points sampled

according to the Merz–Kollman scheme[27] using the Gaussian 03 software package.[28] Charges were fitted to these potentials using the RESP (restrained electrostatic potential) procedure using the antechamber program,[29] which also assigned AMBER atom types to the residues. Missing force-field parameters were estimated from the harmonic frequencies calculated at the same level of theory using the Hess2FF approach.[30,31] AMBER topology and parameter files for these residues are included in the supplementary material.

Six different properties were studied in the various simulations, viz. the radius of gyration, the root-mean-squared deviation (RMSD) from the starting crystal structure, average *B* factors of the various residues, the S–S distances of the cystine disulphide pairs, as well as the hydrogen-bond structure of the active site and around the oxidised amino acid. The properties were obtained with the AMBER ptraj module, analysing trajectories with coordinates saved every 5 ps. The reported values are averages over these 3600 sets of coordinates and uncertainties are the standard deviations over these sets divided by $\sqrt{3600}$.

Construction of CalB M72S

CalB M83I, M129L and W155Q were kind gifts from Novozymes A/S (Bagsvaerd, Denmark). CalB M72S was constructed using site-directed mutagenesis with the plasmid pET-b(+) as template.[32] Mutagenesis was performed using 45 ng template plasmid, 10 pmol of oligonucleotides, 10 nmole of dNTP, 1 U of *Phusion* DNA polymerase (Thermo Fisher Scientific, Waltham, USA) and 10 µl of 5x *Phusion* HF buffer in a final volume of 50 µl. After initial denaturation at 98°C for 30 s, amplification was carried out by 30 cycles at 98° C for 10 s followed by 72° C for 3 minutes and 30 s. Hereafter, D*pn*I digestion of the template DNA was performed before 1 µl of the mixture was inserted by electroporation into *E. coli* Rosetta (DE3) and positive transformants were selected on LB plates containing ampicillin (100 µg/ml) and chloramphenicol (30 µg/ml). The point mutation was verified by DNA sequencing.

Protein expression and purification

For expression of CalB M72S in the periplasmic-space variant in *E. coli*, 1 ml of overnight culture (10 ml in LBCam, Amp) was inoculated into 100 ml of SuperbrothCam, Amp medium. The culture was allowed to reach an OD600 of 0.5 before induction with 1 mM isopropyl β-D-1-thiogalactopyranoside for 24 hours at 16° C. The protein was isolated by osmotic chock after harvesting the cells by centrifugation (3300*g* and 4º C for 15 minutes), by adding 10 ml buffer (30 mM Tris-HCl, 20% sucrose, pH 8) and 20 µl 0.5 M EDTA (final concentration 1 mM), pH 8 for 10 minutes. The supernatant was discarded after a second centrifugation step similar to the first and the cells were re-suspended in 10 ml ice-cold 5 mM $MgSO_4$ and again incubated for 10 minutes. Finally, the periplasmic fraction was isolated by centrifugation of the cells at 21000*g* and 4º C for 15 minutes. The protein was purified on His SpinTrap columns (GE Healthcare) according to the manufacturer's recommendations, followed by a desalting step on PD SpinTrap G-25 columns (GE Healthcare) also according to the manufacturer's recommendations.

Hydrogen-peroxide treatment

Native CalB (filtered Lipozyme® CALB L), as well as CalB M72S, M83I, M129L, and W155Q were diluted to equal concentrations, as determined by absorbance measurements at 280 nm, verified also by Bradford[33] and active-site titration.[16] The enzymes were treated with 0.2 and 2 M H_2O_2 at room temperature and 40°C in a HTMR-131 thermomixer (HLC, Germany; 700 rpm). Enzyme samples (10 µl) were withdrawn after 0–24 h H_2O_2 treatment and were mixed 1:1 with cyclohexane.

Assay of lipase activity

Lipase activity was examined by the esterification of decanoic acid (100 mM) with dodecanol (51 mM), dissolved in cyclohexane. Tetradecane was added to the substrate as internal standard. Samples were withdrawn at appropriate time intervals, diluted with cyclohexane, and the composition was determined using a Varian 430 GC (Varian Instrument group, Walnut Creek, CA, USA). The analytes were separated on a VF-1ms column (15 m length, 0.25 mm inner diameter, 0.25 mm d_f) from Varian Instrument group and was detected with a flame ionisation detector. The column temperature was increased from 90°C to 250°C in 8.5 min, and the temperature of the injector and detector was held at 250° and 300°C, respectively. The retention times were 3.1 and 6.3 min for dodecanol and dodecyl decanoate, respectively.

Immobilization and chemo-enzymatic epoxidation

Native CalB, and the M83I and M129L mutants were immobilized on sieved Accurel® MP 1000 (250–500 μm). The support was wetted with ethanol (3 ml/g) and thereafter loaded with approximately 20 mg enzyme/g support. The support and enzyme mixtures were incubated overnight with shaking. The supernatant was collected and the enzyme preparation dried in a vacuum desiccator. The lipases were adsorbed completely, as determined by measuring the residual activity in the supernatant with the esterification assay described above.

The chemo-enzymatic epoxidation was performed using 5 mg of immobilized enzyme added to 1 g rapeseed methyl ester and 320 μl H_2O_2 (30% w/w) in a 4 ml vial. Incubation was performed in a thermomixer at 40°C, 700 rpm, and samples were withdrawn at appropriate intervals (1–24 h). Samples were centrifuged to remove water, weighted, and the oxirane numbers were measured as described previously.[16] After 24 hours, the substrate and product mixtures were removed from the enzyme beads by pipetting, and substrates were added for a second batch of chemo-enzymatic epoxidation.

Results and Discussion

In order to gain some understanding of the effect of oxidation, we have performed MD simulations of wild-type CalB, the enzyme with one or two oxidised amino-acid residues, and four mutants (16 simulations in total). The enzyme was equilibrated for 0.5 ns and then simulated for 18 ns, during which time we studied six different properties, viz. the radius of gyration, the RMSD from the starting crystal structure, the average *B* factors of the various residues, the S–S distances of the cystine disulphide pairs, as well as the hydrogen-bond structure of the active site and around the oxidised amino acid. The results of this analysis are described in separate sections below. We also constructed four mutants by site-directed mutagenesis and studied their activity and stability.

Radius of gyration

The radius of gyration describes the general size of the protein. It indicates global changes in the shape of the protein. The radii of gyration during the simulations are shown in Figure 3 and the average values over the 18 ns production simulations are listed in Table 1. It can be seen that most of the simulations give average radii of gyration of 18.24–18.27 Å. However, the C216/258 and C293/311 simulations give slightly larger radii of 18.32 and 18.31 Å. This indicates that the oxidations do not have any major impact on the general shape of the protein, except some rather small changes when the cystine disulphide linkages are broken.

For three of the mutants, the radii of gyration are significantly lower than for the wild-type enzyme: For the M129L mutant, it is 18.08 Å, whereas for the M72S and W155Q

mutants it is 18.21–18.22 Å. These changes are caused by the mutations, because the radius of gyration depends on the mass of the various atoms (the moments of inertia).

RMSD

The RMSD shows how much the structure differs from the starting (crystal) structure. The RMSD during the simulations is shown in Figure 4 and Table 1 shows the average over the 18 ns simulations. The flexible loop at the entrance of the active-site cleft, involving residues 140–150, was excluded from the analysis because it showed slow motions even for the wild-type enzyme, which would hide all the other motions of the enzyme. It can be seen that the RMSD shows appreciably larger differences between the various simulations than the radii of gyration. For most of the simulations, including the two wild-type simulations, the RMSD is 0.68–0.80 Å. However, five of the simulations give significantly larger RMSDs of 0.88–1.53 Å (note that the standard error is less 0.001–0.002 Å). These are the three Cys oxidations, as well as the M298 oxidation and the M83I mutation. These five simulations also show some trends or oscillations in the time course of the RMSD, indicating that the simulations are not fully stable. This clearly shows that the Cys oxidations lead to quite large changes in the structure of CalB.

B-factor analysis

Next, we studied the average calculated *B* factor of all residues in the protein, in order to see if there is any increase in the flexibility of certain parts of the structure. The *B* factors are plotted in Figure 5. The plot clearly shows the large flexibility of the solvent-exposed helix formed by residues 140–150 and the adjacent residues 282–290. The average *B* factor over the whole protein, except these two sections, is 15–17 $Å^2$ for all simulations, except the three simulations with Cys oxidations and the M83I mutant, which has slightly higher *B* factors (20–24 $Å^2$). For the M83I mutant, the differences are essentially restricted to a few residues at the start and the end of the enzyme (residues 1–10 and 315–317), probably indicating a variation not induced by the mutation.

On the other hand, the three oxidations of Cys residues give rise to large *B* factors of at least one of the oxidised Cys residues, e.g. by 63 $Å^2$ for Cys 22 (and 250 $Å^2$ for Gln-23), 120 $Å^2$ for both Cys-216 and Cys-258 (and 476 $Å^2$ for Ile-255), as well as 116 and 291 $Å^2$ for Cys-293 and Cys-311. This shows that cleavages of the Cys–Cys links lead to large increases in the flexibility of local environment.

None of the other residue oxidations or mutations lead to any significant increase in the *B* factors of the affected residue (*B* factors of 6–21 $Å^2$, which are within 8 $Å^2$ of the results for the wild-type simulation). However the oxidation of Met-72 leads to an increase in the *B* factor of three neighbouring residues (67–69), by up to 29 $Å^2$. No such effect is seen for the M72S mutant.

S–S bonds

The distance between the two S atoms in the Cys–Cys links after the oxidation indicates how much the cleavage of the Cys–Cys bridges affects the structure. Our results show that the C22/64 and C293/311 oxidations give rise to rather small changes in the structure: The S–S distances increase from 2.04±0.001 Å to 5.29±0.01 and 5.20±0.01 Å, respectively. However, the C216/258 oxidation leads to a major change in the local structure, with a S–S distance of 12.39±0.03 Å. This shows that the two Cys residues have drifted away after the cleavage of the S–S bond.

Hydrogen-bond structure of the active site

Next, we studied the hydrogen-bond structure of the active site in the various simulations. This is probably the most important property, because it shows what effect the oxidations have on the structure of the active site. The results in Table 2 show that there are some differences in the active-site hydrogen bonds. However, the most important interaction, viz. the hydrogen bond between HD1 of His-224 and OD2 of Asp-187 (the atom names follow the convention used in protein data bank crystal structures[34]), shows only small changes between the various simulations: It is present in ~90% of the structures in all simulations and is complemented in ~20% of the structures by a hydrogen bond to the other OD1 atom in Asp-187. On the other hand, there is no hydrogen bond between HG in Ser-105 and NE2 of His-224 in any of the simulations. Instead, HG of Ser-105 forms hydrogen bonds with water (68–86% occupancy). In the WtD simulation, HG of Ser-105 often forms a hydrogen bond to the OD1 atom of the deprotonated Asp-134 residue (24% occurrence). NE2 of His-224 also forms hydrogen bonds with water molecules (51–79% occurrence) in all simulations.

There are some additional differences between the various structures, but only for hydrogen bonds with relatively low occurrence. The C216/258 simulation shows the largest deviations with a new hydrogen bond between the OD2 atom of Asp-187 and HE22 of Gln-193 (62% occurrence), frequent hydrogen bonds between the back-bone H atom of His-224 and water molecules (40% occurrence, respectively), and changed interactions for the O atom of His-224. This simulation, as well as those of oxidised C22/64 and W52 show decreased interactions between the HE22 atom of Gln-191 and the back-bone O atom of Asp-187 (17–28% occupancy, compared to 60% in the WtP simulation. C22/59 also shows an increased occurrence of the hydrogen bond between the back-bone H atom of Glu-188 and the OD1 atom of Asp-187 (59% compared to 22% for WtP). Both WtD and the C293/311 mutant show an increased occurrence of hydrogen bonds between back-bone O atom of Ser-105 and water molecules (109 and 58%). The four mutants do not show any extensive changes in the active-site hydrogen-bond pattern.

Hydrogen bonds around the oxidised residues

Finally, we have compared the hydrogen-bond structure around the affected residues of the native protein (WtP) and the simulation of the oxidised or mutated amino acids. The results are presented in Table 3 with separate sections for each oxidised amino acid or mutation.

For the C22/64 simulation, the oxidation introduces new hydrogen-bond partners (O1, O2, O3, and HO3 atoms in the oxidised Cys residues) that can form hydrogen bonds that of course are not possible in the wild-type enzyme (these atoms are marked in bold face in Table 3). For the atoms that are present in both simulations, there some differences in the occurrence of the hydrogen-bonds (up to 42% units), but no qualitative differences.

However, for the C216/258 simulation, more extensive changes are observed. In particular, hydrogen bonds involving H of Cys-258 disappear and are replaced by new hydrogen bonds involving the oxidised atoms, as well as a hydrogen bond between O of Cys-258 and Gln-231 or water.

Likewise, the C293/311 simulation shows major changes in the hydrogen-bond pattern. First, a new hydrogen bond involving H of Cys-293 and OD1 of Asn-292 appears. Second, a strong hydrogen bond between O of Cys-293 with HE22 of Gln-291 is replaced by hydrogen bonds to water molecules. Third, a strong hydrogen bond between H of Cys-311 and O of Glu-294 is replaced by weaker and more occasional hydrogen bonds with water. This shows that the oxidised Cys residues become more water-exposed. In addition, several new hydrogen bonds are formed with the oxidised atoms of the two Cys residues.

Among the four Met oxidations, the oxidised OS atoms of Met-72 and Met-298 form 1–3 hydrogen bonds with water molecules. The Met-72 simulation also shows other changes in

the hydrogen-bond structure, involving the H and O atoms. On the other hand, the oxidations of Met-83 and 129 do not lead to any significant changes in the hydrogen-bond pattern and no interactions with the new OS atoms are observed. The reason for this is that these two residues are deeply buried in the protein (cf. Figure 2).

The oxidation of the Trp residues gives rise to a new OH group (HOZ3), which forms hydrogen bonds in all three simulations. However, the occurrence of the hydrogen bonds is varying, reflecting the solvent-accessibility of the group (Trp-52 is buried in the protein, Trp-65 is more solvent exposed, but the CZ3 atom is directed into the protein, whereas Trp-155 is on the surface of the protein with CZ3 directed into the solvent, cf. Figure 2). For the other atoms in the oxidised Trp residues, there are only rather small differences, the largest being the hydrogen bond between HE1 of Trp-155 and O of Leu-228 (the occurrence decreases from 47 to 13%).

The M72S mutant gives rise to two new hydrogen bonds involving the OH group of the Ser residue and water molecules. In addition, the occurrence of the hydrogen bond between H and O of Pro-68 increases from 19 to 50%. The M83I mutant shows only a fairly small decrease in the H atom and O of Thr-83 (from 49 to 28% occurrence), whereas the M129L mutant does not show any significant changes in the hydrogen-bond pattern. On the other hand, the W155Q mutation leads to quite extensive changes in the hydrogen-bond structure: The hydrogen bond between the Trp HE1 atom and O Gln-291 is replaced by four hydrogen bonds between the Gln OE1 and HE2 atoms and water, OD of Asp145, and O of Gln-291.

Altogether, the results of the MD simulations indicate that the oxidations of Met and Trp residues have a quite restricted influence on the structure and activity of CalB. On the other hand, oxidations of the Cys residues, implying cleavage of the Cys–Cys linkages, have much larger effects on the enzyme structure and dynamics. In particular, oxidation of the Cys-216/258 pair, and to a smaller extent also the Cys-22/64 pair, is predicted to severely perturb the structure of the active site and therefore probably decrease the activity.

Activity and stability of CalB mutants

To gain further understanding of the influence of oxidised amino acid residues on enzyme activity and stability, some point-mutated variants of CalB were produced on the basis of the MD simulations and our previous studies.[16,17] Since the Cys–Cys linkages are important for the stability of the protein, we concentrated on the Met and Trp residues. The single-point mutation of the CalB residue Met-72 has been constructed before by Patkar et al.[35] using leucine as substituent. They reported that this mutant displayed a slightly higher oxidative stability, but at expense of its thermostability. Estell et al.[36] have suggested that replacing Met with Ala or Ser instead of Leu might generate a more active enzyme. As computer modelling indicates that Ser fits better than Ala at this position in CalB (data not shown), we decided to produce the CalB M72S variant. Three additional CalB mutants, M83I, M129L, and W155Q, were provided in purified form by Novozymes (Bagsvaerd, Denmark).

All enzyme variants showed a lower specific activity than native CalB when assayed for the esterification of decanoic acid with dodecanol; the W155Q mutant having the lowest (5% of native) and M83I the highest (58%) activity, see Table 4. Based on residual activities for the enzymes after incubation with H_2O_2 at room temperature and 40° C, M83I seems to have a somewhat higher thermostability, but a slightly lower oxidative stability than the native enzyme (Table 4). On the other hand, M72S showed no activity after treatment with 0.2 M H_2O_2 at 40°C for 24 h, but it still had 51% activity after 24 h incubation at 2 M H_2O_2 at room temperature. This decrease in thermostability is consistent with the M72L variant investigated by Patkar et al.[35] The M129L and W155Q mutants had a rather low thermostability (8–9% residual activity after 24 h at 40° C, but at room temperature the latter mutant had almost the same stability in 2 M H_2O_2 as the native protein, whereas the M129L mutant showed only 18% residual activity (Table 4). The M83I and M129L mutants had higher residual activity

than native enzyme after incubation at 40° C with 2 M H_2O_2 (37 and 41%, respectively, versus 24% for native enzyme after 4 h).

Native CalB, and the M83I and M129L mutants were immobilized were immobilized by adsorption on Accurel® MP 1000 and tested as catalysts in the chemo-enzymatic epoxidation of rapeseed methyl ester. W155Q was not considered active enough and the in-house constructed M72S had too low specific activity to justify production of the amount needed for immobilization. For chemo-enzymatic epoxidation, the native enzyme was the most active as can be seen in Table 5. All enzymes showed only minor activity when reused, with native CalB having slightly higher remaining activity than the mutants.

As mentioned above, the same four mutants were also studied by MD simulations. The results in Tables 1–3 and Figures 3–5 show that the MD simulations predict rather small changes in these mutants compared to the native enzyme: The M83I mutant showed an increased RMSD from the crystal structure, but mainly of the two ends of the enzyme, which is not expected to affect the activity of the enzyme significantly. Neither of the mutants showed any large changes in the hydrogen-bond structure of the active site, besides a 26%-unit decrease in the occurrence of the hydrogen bond between H of Gln-106 and OG of Ser-105 in the M83I mutant. Likewise, we see only small changes in the hydrogen-bond pattern around the mutated residues, besides hydrogen bonds involving atoms directly involved in the mutations and a 21–31%-unit change in the occurrence of a hydrogen bond involving the back-bone H atom of the mutated residue for the M72S and M83I mutations.

Comparing these results with those obtained by the experimental studies, we can conclude that the both studies agree that the changes are only small and quantitative. The largest observed difference is the low activity of the W155Q, which is not reflected by any major changes in the hydrogen bonds in the active site. Apparently, a study of the hydrogen bonds is too simple to catch subtle changes in the activity of the enzyme (a 95% decrease in the activity corresponds to a increase in the activation barrier of only 7 kJ/mol). It is possible that simulations of an enzyme–substrate complex instead would yield more information regarding the activity of the mutants,[37] but it is likely that much more sophisticated methods, involving direct calculations of activation barriers would be needed, and it is still not certain that the accuracy such methods would be enough to correctly predict changes in the activation energy of 7 kJ/mol or less. On the other hand, both experiments and simulations indicate that the Met and Trp residues are not the main cause of enzyme inactivation. Instead, oxidation of the Cys residues seems to be most detrimental for the activity.

Conclusions

Based on the earlier reports on oxidative deactivation of CalB in the presence of H_2O_2, we have in this study performed MD simulations of CalB in its native state and with one or two oxidised amino acids. The oxidised amino acids were selected from a mass spectrometry-based investigation, showing which amino acids are most prone to be oxidised.[17] The results show that oxidations and cleavages of all three cystine disulphide bridges gave extensive changes in the local structure of the protein, as indicated by the RMSD from the crystal structure, even if the two residues drifted away only in the case of the C216/258 pair. The latter simulation also gave rise to rather large changes in the hydrogen-bond structure of the active site and a significant increase in the radius of gyration of the enzyme. We have also looked at the hydrogen-bond structure around the oxidised residues, showing that the new polar atoms that arise through the oxidation often form hydrogen bonds with the surroundings, especially if the residues are solvent exposed. The latter residues often show changes in the hydrogen bonds for the other atoms in the residue as well, but this mainly reflects the increased flexibility of the residue, rather than any extensive changes in the conformation.

In accordance with the results from the MD simulations, single-point mutations of

methionine residues had a modest effect on enzyme activity. One variant, M83I, was more stable than the native enzyme when exposed to H_2O_2 at some conditions. The tryptophan variant (W155Q), on the other hand, showed a severe decrease in activity towards the tested substrates. Unfortunately, the variants had neither significantly increased stability towards H_2O_2 nor improved activity or stability during chemo-enzymatic epoxidation. MD simulations of the same mutations indicated small changes in the structure of the protein, but were unable to predict the observed subtle changes in enzyme activity.

In conclusion, the MD simulations provide clues on the possibilities to mutate certain oxidation sensitive residues without having significant impact on the structure and shape of the protein, but single-point mutations of several of those residues did not notably improve the stability of CalB. Moreover, the specific activity of the enzyme was compromised. As the cleavage of the cystine bonds appears to be the major cause of activity loss, it seems difficult to obtain an active and more stable enzyme simply by site-directed mutagenesis. Nevertheless some approaches could be attempted. The Cys residues themselves need to be preserved because the linkages are important for the stability, but they could be made less solvent accessible by mutating neighbouring residues to bulkier groups. Another mutation strategy could be to protect sensitive areas by incorporation of oxidation-sensitive amino acids (e.g. Met residues) to function as protective residues; Met residues on the surface can often be oxidised without affecting enzyme activity.[16,38,39]

On the other hand, biocatalyst engineering by immobilization of the enzyme on a suitable support may provide a simpler approach for stabilization. Immobilization of CalB on hydrophobic octadecyl Sepabeads[40] and styrene-divinylbenzene beads[41] has been shown to give increased stability towards oxidation by H_2O_2, which could be attributed to shielding of sensitive residues.[40] However, as H_2O_2 is the substrate for the enzyme in chemo-enzymatic epoxidation, it is essential that the active site of the immobilized enzyme is still accessible for H_2O_2 . This remains to be tested as well as the economic feasibility of the preparation. In conclusion, the results presented here can lay the basis for further stabilization experiments as well as studies to further elucidate the effect of oxidation on biocatalyst activity and stability.

Acknowledgements

This investigation has been supported by grants from the Swedish research council (project 2010-5025), from the FLÄK research school in pharmaceutical science, from the Crafoord foundation, and from the Wenner-Gren foundation. It has also been supported by computer resources of Lunarc at Lund University, NSC at Linköping University, C3SE at Chalmers University of Technology, and HPC2N at Umeå University. Jesper Brask, Novozymes (Bagsvaerd, Denmark) is acknowledged for providing M83I, M129L and W155Q. M.Sc. student Camilla Melin Fürst is thanked for performing activity and stability measurements, and a grant to support her from Novo Scholarship Programme (Novozymes A/S and Novo Nordisk A/S, Bagsvaerd, Denmark) is also acknowledged.

References

1 Bummer, P. M.; Kuppenol, S. Chemical and physical considerations in protein and peptide stability. *Drugs Pharmaceut. Sci.* **2000**, *99*, 5-69

2 Buisman, G. J. H. Biodegradable binders and cross-linking agents from renewable resources. *Surf. Coat. Int.* **1999**, *82*, 127-130

3 Benaniba, M. T.; Belhaneche-Bensemra, N.; Gelbard, G. Stabilization of PVC by epoxidized sunflower oil in the presence of zinc and calcium stearates. *Polym. Degrad. Stab.* **2003**, *82*, 245-249

4 Warwel, S.; Bruse, F.; Demes, C.; Kunz, M.; Klaas, M. R. Polymers and surfactants on the basis of renewable resources. *Chemosphere* **2001**, *43*, 39-48

5 Orellana-Coca, C.; Törnvall, U.; Adlercreutz, D.; Mattiasson, B.; Hatti-Kaul, R. Chemo-enzymatic epoxidation of oleic acid and methyl oleate in solvent-free medium. *Biocatal. Biotransform.* **2005**, *23*, 431-437

6 Orellana-Coca, C.; Camocho, S.; Adlercreutz, D.; Mattiasson, B.; Hatti-Kaul, R. Chemo-enzymatic epoxidation of linoleic acid: parameters influencing the reaction. *Eur. J. Lipid Sci. Technol.* **2005**, *107*, 864-870

7 Orellana-Coca, C.; Billakanti, J.; Mattiasson, B.; Hatti-Kaul, R. Lipase mediated simultaneous esterification and epoxidation of oleic acid for the production of alkylepoxystearates. *J. Mol. Catal. B* **2007**, *44*, 133-137

8 Björkling, F.; Frykman, H.; Godtfredsen, SE.; Kirk, O. Lipase catalyzed synthesis of peroxycarboxylic acids and lipase mediated oxidations. *Tetrahedron* **1992**, *48*, 4587-4592

9 Patkar, S.; Björkling, F.; Zundell, M.; Schulein, M.; Svendsen, A.; Hansen, H. H.; Gormsen, E. Purification of two lipases from *Candida antarctica* and their inhibition by various inhibitors. *Ind. J. Chem.* **1992**, *32B*, 76-80

10 Andersson, E. M.; Larsson, K. M.; Kirk, O. One biocatalyst – many applications: The use of *Candida antarctica* lipase in organic synthesis. *Biocatal. Biotransform.* **1998**, *16*, 181-204

11 Uppenberg, J.; Hansen, M. T.; Patkar, S.; Jones, T. A. Sequence, crystal structure determination and refinement of 2 crystal forms of lipase-b from Candida antarctica. *Structure* **1994**, *2*, 293-308

12 Uppenberg, J.; Ohrner, N.; Norin, M.; Hult, K.; Kleywegt, G. J.; Patkar, S.; Waagen, V.; Anthonsen, T.; Jones, T. A. Crystallographic and molecular-modeling studies of lipase B from *Candida antarctica* reveal a stereospecificity pocket for secondary alcohols. *Biochemistry* **1995**, *34*, 16838-16851

13 Martinelle, M.; Holmqvist, M.; Hult, K. On the interfacial activation of *Candida antarctica* lipase-A and lipase-B as compared with *Humicola-lanuginosa* lipase. *Biochim. Biophys. Acta* **1995**, *1258*, 272-276

14 Blank, K.; Morfill, J.; Gumpp, H.; Gaub, H. E. Functional expression of *Candida antarctica* lipase B in *Escherichia coli*. *J Biotechnol.* **2006**, *125*, 474-483

15 Törnvall, U.; Orellana-Coca, C.; Hatti-Kaul, R.; Adlercreutz, D. Stability of immobilized *Candida antarctica* lipase B during chemo-enzymatic epoxidation of fatty acids. *Enzyme Microb. Technol.* **2007**, *40*, 447-451

16 Törnvall, U.; Hedtröm. M.; Schillén, K.; Hatti-Kaul, R. Structural, functional and chemical changes in *Pseudozyma antarctica* lipase B on exposure to hydrogen peroxide. *Biochemie*, **2010**, *92*, 1867-1875.

17 Törnvall, U.; Melin Furst, C.; Hatti-Kaul, R.; Hedström, M. Mass spectrometric analysis of peptides from an immobilized lipase: focus on oxidative modifications. *Rapid Communications in Mass Spectrometry* **2009**, *23*, 2959-2964

18 Bas, D. C.; Rogers, D. M.; Jensen, J. H.Very fast prediction and rationalization of pKa values for protein-ligand complexes, *Proteins*, **2008**, *73*, 765-783.

19 Case, D.A.; Cheatham, III, T.E.; Darden, T.; Gohlke, H.; Luo, R.; Merz, Jr., K.M.; Onufriev, A.; Simmerling, C.; Wang B.; Woods, R. The Amber biomolecular simulation programs. *J. Comput. Chem.* **2005**, *26*, 1668-1688

20 Wu, X.; Brooks, B.R. Self-guided Langevin dynamics simulation method. *Chem. Phys. Lett.* **2003**, *381*, 512-518

21 Berendsen, H.J.C.; Postma, J.P.M.; van Gunsteren, W.F.; DiNola, A.; Haak, J.R. Molecular dynamics with coupling to an external bath. *J Chem Phys*, **1984**, *81*, 3684–3690

22 Darden, T.; York, D.; Pedersen, L. Particle mesh Ewald: An *N*log(*N*) method for Ewald sums in large systems. *J. Chem. Phys.* **1993**, *98*, 10089-10092

23 Ryckaert, J. P.; Ciccotti, G.; Berendsen, H. J. C. Numerical integration of the Cartesian equations of motion of a system with constraints: molecular dyanmics of *n*-alkanes. *J. Comput. Phys.*, **1977**, 23, 327-341

24 Hornak, V.; Abel, R.; Okur, A.; Strockbine, B.; Roitberg, A.; Simmerling, C. Comparison of multiple Amber force fields and development of improved protein backbone parameters. *Proteins* **2006**, *65*, 712-725.

25 Jorgensen, W. L.; Chandrasekhar, J.; Madura, J. D.; Impey, R. W.; Klein, M. L. Comparions of

simple potential functions for simulating liquid water *J. Chem. Phys.*, **1983**, *79*, 926-935.
26 Schey, K. L.; Finley, E. L. Identification of peptide oxidation by tandem mass spectrometry. *Acc. Chem. Res*. **2000**, *33*, 299-306.
27 Besler, B. H.; Merz, K. M.; Kollman, P. A. Atomic charges derived from semiempirical methods. *J. Comput. Chem.* **1990**, *11*, 431-439.
28 Frisch, M. J.; Trucks, G. W.; Schlegel, H. B.; Scuseria, G. E.; Robb, M. A.; Cheeseman, J. R.; Montgomery, Jr., J. A.; Vreven, T.; Kudin, K. N.; Burant, J. C.; Millam, J. M.; Iyengar, S. S.; Tomasi, J.; Barone, V.; Mennucci, B.; Cossi, M.; Scalmani, G.; Rega, N.; Petersson, G. A.; Nakatsuji, H.; Hada, M.; Ehara, M.; Toyota, K.; Fukuda, R.; Hasegawa, J.; Ishida, M.; Nakajima, T.; Honda, Y.; Kitao, O.; Nakai, H.; Klene, M.; Li, X.; Knox, J. E.; Hratchian, H. P.; Cross, J. B.; Bakken, V.; Adamo, C.; Jaramillo, J.; Gomperts, R.; Stratmann, R. E.; Yazyev, O.; Austin, A. J.; Cammi, R.; Pomelli, C.; Ochterski, J. W.; Ayala, P. Y.; Morokuma, K.; Voth, G. A.; Salvador, P.; Dannenberg, J. J.; Zakrzewski, V. G.; Dapprich, S.; Daniels, A. D.; Strain, M. C.; Farkas, O.; Malick, D. K.; Rabuck, A. D.; Raghavachari, K.; Foresman, J. B.; Ortiz, J. V.; Cui, Q.; Baboul, A. G.; Clifford, S.; Cioslowski, J.; Stefanov, B. B.; Liu, G.; Liashenko, A.; Piskorz, P.; Komaromi, I.; Martin, R. L.; Fox, D. J.; Keith, T.; Al-Laham, M. A.; Peng, C. Y.; Nanayakkara, A.; Challacombe, M.; Gill, P. M. W.; Johnson, B.; Chen, W.; Wong, M. W.; Gonzalez, C.; and Pople, J. A. Gaussian 03, Gaussian, Inc., Wallingford CT, **2004**.
29 Bayly, C. I.; Cieplak, P.; Cornell, W. D.; Kollman, P. A. A well-behaved electrostatic potential based method using charge restraints for deriving atomic charges: The RESP model. *J. Phys. Chem.* **1993**, *97*, 10269-10280.
30 Seminario, J. M. Calculation of intramolecular force fields from second-derivative tensors, *Int. J. Quantum Chem*. **1996**, *60*, 1271-1277.
31 Nilsson, K.; Lecerof, D.; Sigfridsson; E.; Ryde, U. An automatic method to generate force-field parameters for hetero-compounds. *Acta Crystallogr. D*, **2003**, *59*, 274-289.
32 Wittrup Larsen, M.; Hult K.; Bornscheuer U. Expression of *Candida antarctica* lipase B in *Pichia pastoris* and various *Escherichia coli* systems. *Protein Express. Purif.* **2008**, *62*, 90-97
33 Bradford M.M. Rapid and sensitive method for the quantitation of microgram quantities of protein utilizing the principle of protein-dye binding. *Anal. Biochem.* **1976**, *72*, 248–254
34 http://www.wwpdb.org/documentation/format33/v3.3.html
35 Patkar, S.; Vind, J.; Kelstrup, E.; Christensen, M.W.; Svendsen, A.; Borch, K.; Kirk, O. () Effect of mutations in *Candida antarctica* B lipase. *Chem. Phys. Lipids* **1998**, *93*, 95-101.
36 Estell, D.A.; Graycar, T.P.; Wells, J.A. Engineerng an enzyme by site-directed mutagenesis to be resistant to chemical oxidation. *J. Biol. Chem.* **1985**, *260*, 6518-6521
37 Karmerlin, S. C. L.; Warshel, A. The empirical valence bond model: theory and applications. *WiRE: Comp. Mol. Sci*. **2011**, *1*, 30-45.
38 Levine, R.; Berlett, B.S.; Moskovitz, J.; Mosoni, L.; Stadtman, E.R. Methionine residues may protect proteins from critical oxidative damage. *Mech. Ageing Dev.* **1999**, 107. 323-332.
39 Davies, M.J. The oxidative environment and protein damage. *Biochim. Biophys. Acta*. **2005**, 1703, 93-109.
40 Hernandez, K.; Fernandez-Lafuente, R. Lipase B from Candida antarctica immobilized on octadecyl Sepabeads: A very stable biocatalyst in the presence of hydrogen peroxide *Process Biochem.* **2011**, *46*, 873-878.
41 Hernandez, K.; Garcia-Galan, C.; Fernandez-Lafuente, R. Simple and efficient immobilization of lipase B from Candida antarctica on porous styrene-divinylbenzene beads *Enz. Microb. Tech.* **2011**, *49*, 72-78.

Table 1. Average radii of gyration (Å) and RMSD from the crystal structure (Å) for the various simulations over the 18 ns simulations.

	radius of gyration	RMSD
WtD	18.240±0.001	0.760±0.001
WtP	18.254±0.001	0.770±0.002
C22/64	18.271±0.001	**0.883**±0.002
C216/258	**18.321**±0.001	**1.530**±0.002
C293/311	**18.305**±0.001	**1.122**±0.001
M72	18.273±0.001	0.750±0.001
M83	18.266±0.001	0.778±0.001
M129	18.247±0.001	0.732±0.001
M298	18.260±0.001	**0.950**±0.002
W52	18.261±0.001	0.702±0.001
W65	18.270±0.001	0.770±0.001
W155	18.237±0.001	0.797±0.002
M72S	18.222±0.001	0.745±0.001
M83I	18.260±0.001	**0.911**±0.002
M129L	18.084±0.001	0.737±0.001
W155Q	18.207±0.001	0.679±0.001

Table 2. Hydrogen bonds in the active site for the various simulations. Listed are hydrogen bonds involving Ser-105, Asp-187, and His-224 with an occurrence larger than 10% in at least one of the simulations. An hydrogen bond is judged to be present in a snapshot if the donor–acceptor distance is less than 3.0 Å and the donor–H–acceptor angle is larger than 120°. The hydrogen bonds are described by the involved H donor and acceptor atoms with atom names following PDB conventions.[34] The listed occurrences are simply the percentage of the 3600 snapshot in which the hydrogen bond is found. Water molecules can have more than 100% of occurrence because more than one water molecule can form hydrogen bonds to the same atom in a specific snapshot. Differences compared to the WtP simulation larger than 20% units are highlighted in bold face.

Donor	Acceptor	WtP	WtD	C22	C216	C293	M72	M83	M129	M283	W52	W65	W155	M72S	M83I	M129L	W155Q
H Ser105	O Phe131	31	35	37	40	40	32	29	35	29	32	33	32	40	24	26	36
H Gln106	OG Ser105	87	75	84	74	81	88	85	88	74	88	85	83	84	**61**	86	82
HE21 Thr57	OG Ser105		2	**27**													
Wat	OG Ser105	3	**36**		15	8	4	8	3	15	5	7	6	9	13	4	8
HG Ser105	OD1 Asp134		24														
HG Ser105	Wat	84	68	80	85	74	85	81	87	76	81	83	85	76	76	85	76
H Gly108	O Ser105	22	22	22	29	23	20	20	21	24	18	23	12	24	24	26	22
Wat	O Ser105	29	**109**	5	24	**58**	30	32	37	23	28	25	14	21	23	24	33
H Asp187	O Ala185		1		8	4	5	3	4	0	8	7	2	5	3	2	4
H Glu 188	OD1 Asp187	22	16	**59**	41	21	21	17	17	26	17	26	17	40	27	33	23
H Ile189	OD1 Asp187	89	91	83	83	85	86	90	87	90	91	87	82	77	76	74	89
H Val190	OD1 Asp187	80	76	87	79	86	80	86	80	80	81	86	90	91	90	91	86
HD1 His224	OD1 Asp187	16	14	19	**38**	26	15	25	19	15	14	23	17	18	20	18	21
Wat	OD1 Asp187	6	7	2			7	1	10	2	5	0		0		0	0
HE22 Gln193	OD2 Asp187		0	0	**62**	0		0	0	0	0	0					0
HD1 His224	OD2 Asp187	90	86	91	84	85	91	88	91	90	89	89	89	93	88	93	91
Wat	OD2 Asp187	99	98	100	**129**	97	98	99	98	99	102	98	99	98	98	104	94
HE22 Gln191	O Asp187	60	65	**28**	**22**	45	60	62	63	72	**17**	35	70	41	71	56	62
Wat	O Asp187	97	96	**126**	**143**	111	101	100	96	93	97	82	93	117	92	99	92
H His224	OE2 Glu188			1	1	1					0	0	0	2	0	3	7
H His224	Wat	10	9	8	**40**	8	13	14	10	3	12	7	5		1		
Wat	NE2 His224	71	66	77	51	68	72	67	71	64	70	68	79	72	68	78	72
HE1 Trp104	O His 224	47	50	41	**3**	55	50	42	44	45	53	41	39	43	38	44	49
Wat	O His 224				**64**												

Table 3. Hydrogen-bond structure involving the oxidised residues in the simulations of the WtP protein and the various oxidised residues (Ox). Only hydrogen bonds with occurrences above 10% in at least one of the simulations are listed. Distances are average distances in Å over the simulations in which the hydrogen bond is present. Donor and acceptor atoms that are present only in the oxidised residue are marked in bold face. Likewise, differences in occurrence between the WT and oxidised simulations larger than 20% units are also marked in bold face.

Ox simulation	donor	acceptor	occurrence		distances	
			Ox	WtP	Ox	WtP
C22/64	H Cys22	Wat	**42**	**18**	2.89	2.89
	H Ala25	**O2 Cys22**	13		2.87	
	WAT	**O2 Cys22**	11		2.79	
	HO3 Cys22	O Ala25	72		2.63	
	HO3 Cys22	WAT	18		2.68	
	Wat	O Cys22	**65**	**42**	2.78	2.76
	H Cys64	O Ile34	**21**	**63**	2.92	2.89
	HO3 Cys64	O Ile34	96		2.67	
	H Leu36	O Cys64	80	91	2.86	2.83
C216/258	H Cys216	O Ala212		81		2.85
	H Gly254	**O1 Cys216**	6		2.89	
	WAT	O Cys216	44		2.78	
	H Cys258	OD1 Asp257	17		2.86	
	Wat	**O1 Cys258**	53		2.79	
	Wat	**O2 Cys258**	53		2.79	
	HO3 Cys258	Wat	36		2.68	
	HE21 Gln231	O Cys258	5		2.85	
	HE22 Gln231	O Cys258	28		2.84	
	Wat	O Cys258	50		2.78	
C293/311	H Cys293	OD1 Asn292	43		2.83	
	Wat	**O1 Cys293**	99		2.79	
	Wat	**O2 Cys293**	90		2.79	
	Wat	**O3 Cys293**	10		2.86	
	HO3 Cys293	Wat	94		2.68	
	HE22 Gln291	O Cys293	**2**	**80**	2.86	2.83
	Wat	O Cys293	86		2.77	
	H Cys311	O Glu294		89		2.83
	H Cys311	Wat	30		2.89	
	Wat	**O1 Cys311**	47		2.79	

	Wat	**O2 Cys311**	50		2.79	
	HO3 Cys311	Wat	95		2.68	
	HH21 Arg309	O Cys311	8		2.84	
	Wat	O Cys311	**53**	**99**	2.77	2.78
M72	H Met72	O Pro68	1	19	2.92	2.91
	H Met72	Wat	**47**		2.89	
	Wat	**OS Met72**	208		2.69	
	HE21 Gln106	O Met72	85	80	2.84	2.85
	HG Ser153	O Met72	**83**	**62**	2.79	2.81
M83	H Met83	O Thr80	38	49	2.88	2.88
	H Ile87	O Met83	74	52	2.87	2.90
M129	H Met129	O Val101	65	66	2.89	2.88
	H Thr103	O Met129	46	45	2.90	2.90
	HG1 Thr103	O Met129	6	13	2.86	2.87
M298	H Met298	OE1 Gln77	70	85	2.86	2.84
	Wat	**OS Met298**	253		2.70	
	H Ala301	O Met298	76	79	2.87	2.86
	H Arg302	O Met298	26	29	2.89	2.91
W52	H Trp52	OD1 Asn51	90	91	2.83	2.83
	HE1 Trp52	O Leu228	**13**	**47**	2.90	2.88
	HOZ3 Trp52	O Leu55	24		2.77	
	H Ser56	O Trp52	29	29	2.90	2.90
	HG Ser56	O Trp52	97	95	2.71	2.70
W65	H Trp65	O Thr21	84	87	2.86	2.85
	HE1 Trp65	Wat	36	49	2.90	2.88
	Wat	**OZ3 Trp65**	51		2.81	
	HOZ3 Trp65	O Pro63	64		2.75	
	HOZ3 Trp65	Wat	20		2.79	
	H Thr21	O Trp65	35	37	2.91	2.91
	Wat	O Trp65	20	28	2.80	2.80
W155	H Trp155	O Ala151	44	40	2.89	2.90
	HE1 Trp155	O Ser150	14	8	2.90	2.90
	HE1 Trp155	O Gln291	69	82	2.85	2.83
	Wat	**OZ3 Trp155**	73		2.81	
	HOZ3 Trp155	OD1 Asp145	97		1.62	
	Wat	O Trp155	70	85	2.77	2.77

M72S	H Met/Ser72	O Pro68	**50**	**19**	2.89	2.91
	Wat	**OG Ser72**	61		2.82	
	HG Ser72	Wat	44		2.77	
	HE21 Gln106	O Met/Ser72	87	80	2.84	2.85
	HG Ser153	O Met/Ser72	69	62	2.82	2.81
M83I	H Met/Ile83	O Thr80	**28**	**49**	2.88	2.88
	H Ile87	O Met/Ile83	63	52	2.89	2.90
M129L	H Met/Leu129	O Val101	76	66	2.87	2.88
	H Thr103	O Met/Leu129	59	45	2.89	2.90
	HG1 Thr103	O Met/Leu129	19	13	2.86	2.87
W155Q	H Trp/Gln155	O Ala151	61	40	2.89	2.90
	HE1 Trp155	O Gln291		82		2.83
	Wat	**OE1 Gln155**	146		2.76	
	HE21 Gln155	OD1 Asp145	39		2.84	
	HE21 Gln155	OD2 Asp145	26		2.84	
	HE22 Gln155	O Gln291	79		2.84	
	Wat	O Trp/Gln155	83	85	2.77	2.77

Table 4. Specific activity of native CalB and four mutants, as well as residual activity after 24 h incubation in presence of hydrogen peroxide.

	Specific activity (μmol/min/mg)	Residual activity (%) 0.2 M H_2O_2, 40° C	Residual activity (%) 2 M H_2O_2, room temperature
CalB	190.8	75	56
M72S	25.5	0	51
M83I	111.3	85	47
M129L	100.1	9	18
W155Q	10.1	8	54

Table 5. Conversion (%) of double bonds during chemo-enzymatic epoxidation of rapeseed methyl ester using native CalB and the M83I and M12L mutants, respectively, immobilized on Accurel® MP 1000.

	Fresh enzyme, 3h	Fresh enzyme, 24h	Reused enzyme, 24h
CalB native	18.7	52.1	2.8
M83I	13.7	32.8	1.4
M129L	14.7	29.4	1.2

Figure 1. Schematic view of the epoxidation reaction catalysed by lipases.

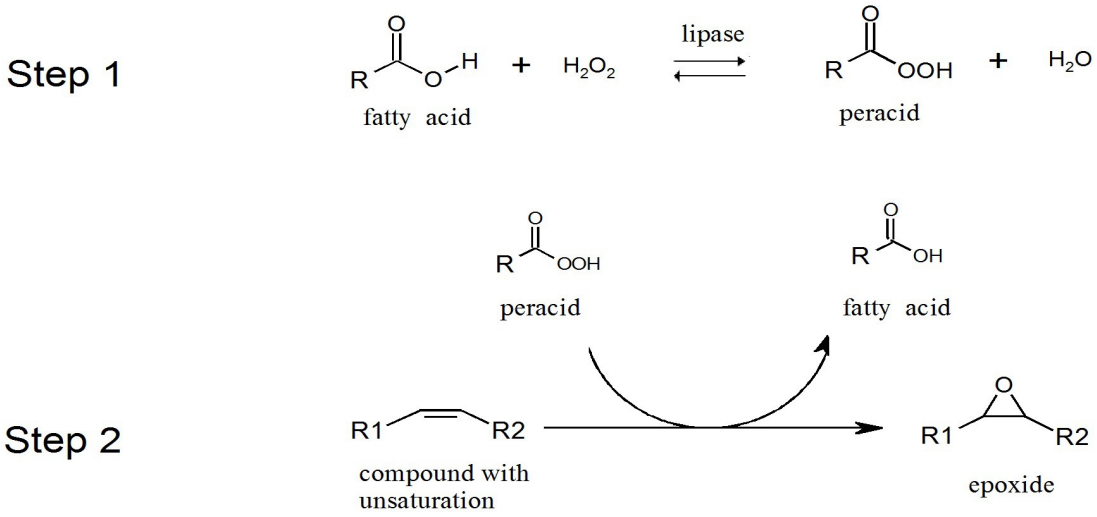

Figure 2. CalB from two different angles with the oxidised residues as well as the catalytic triad marked. A semi-transparent surface of the protein is shown, highlighting the solvent-accessibility of the oxidised residues.

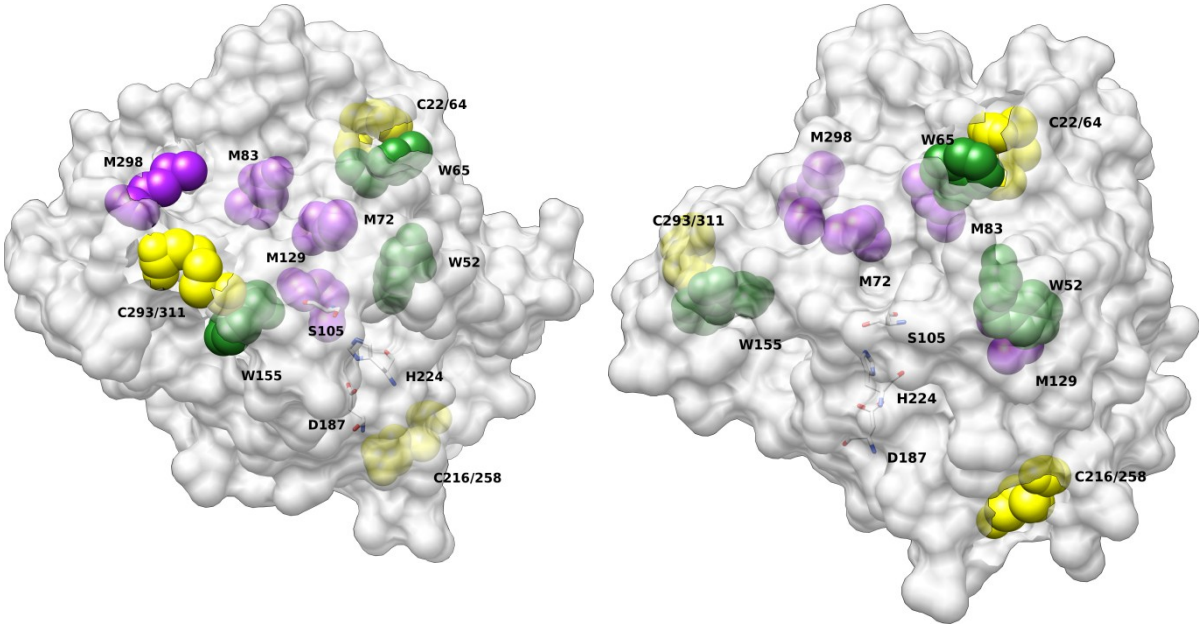

Figure 3. Radii of gyration as a function of time for the various simulations.

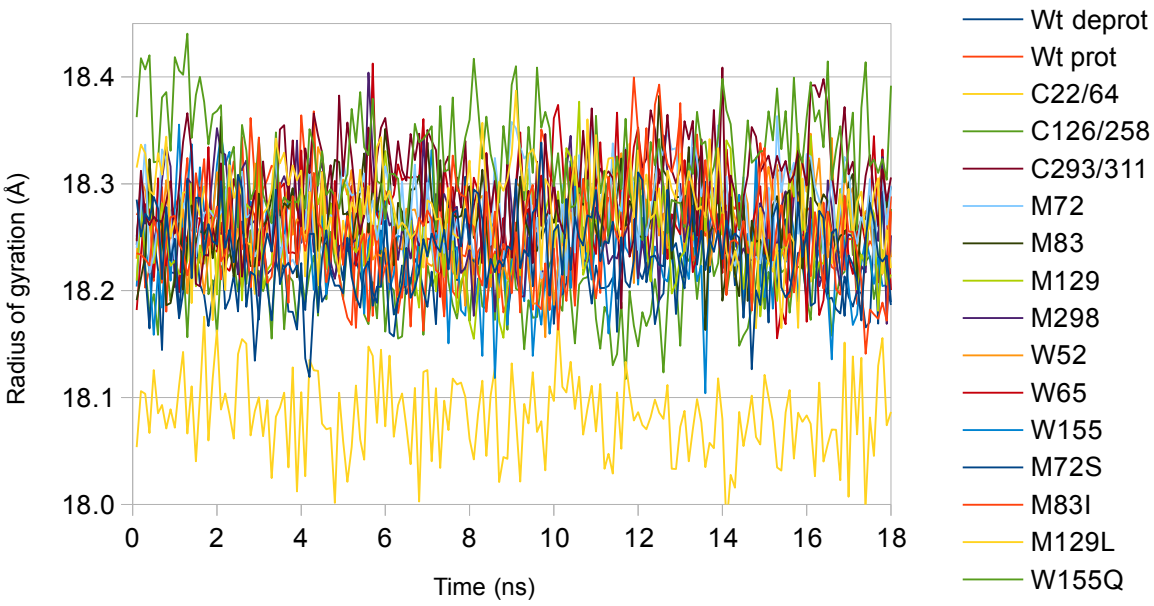

Figure 4. RMSD with respect to the crystal structure as a function of time for the various simulations.

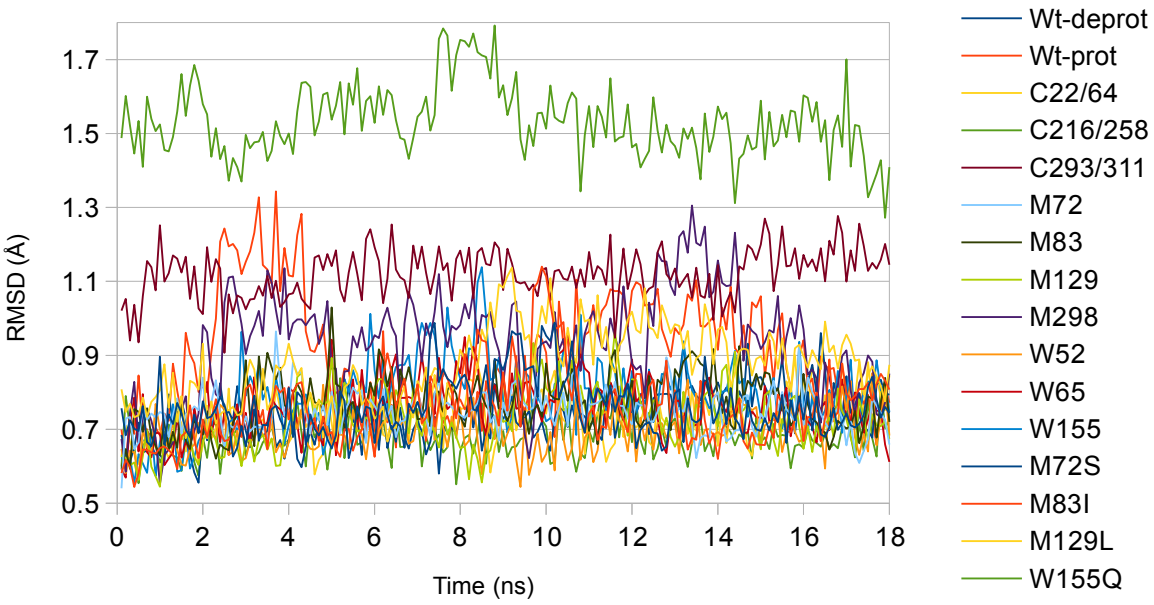

Figure 5. *B* factors for the various residues in CalB calculated over the 18 ns MD simulations. A few large peaks have been truncated to emphasize the typical values.

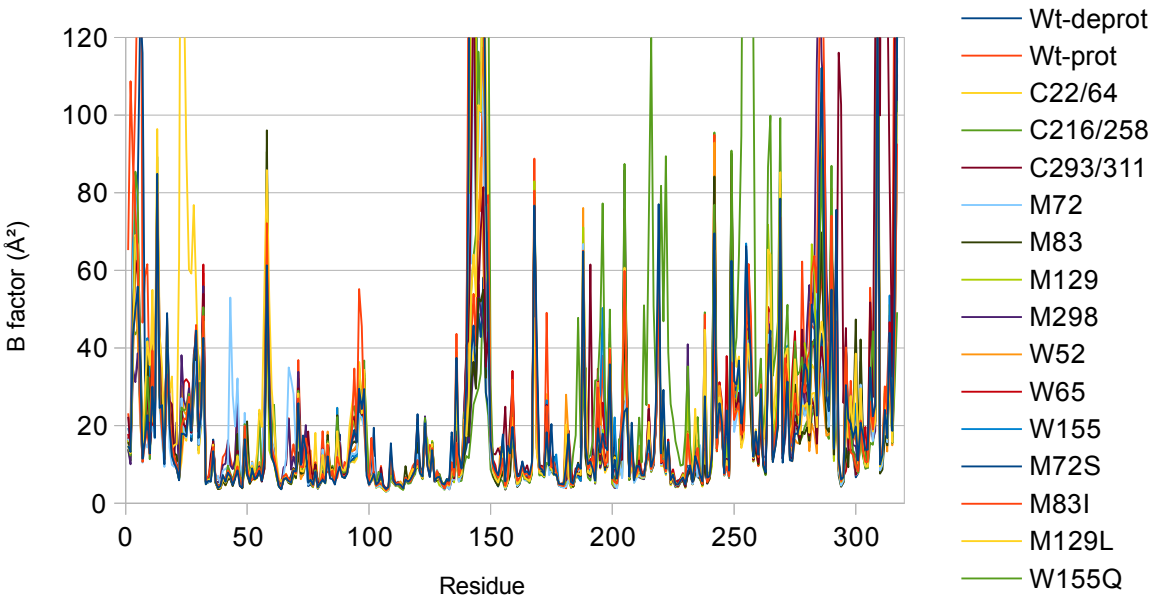

For Table of contents use only

Amino acid oxidation of Candida antarctica lipase B studied by molecular dynamics simulations and site-directed mutagenesis

Mehdi Irani, Ulrika Törnvall, Samuel Genheden, Marianne Wittrup Larsen, Rajni Hatti-Kaul, Ulf Ryde